Optical pulse compression reflectometry: proposal and proof-of-concept experiment

Weiwen Zou,* Shuo Yang, Xin Long, and Jianping Chen

State Key Lab of Advanced Optical Communication and System, Department of Electronic Engineering, Shanghai Jiao Tong University, 800 Dongchuan Road, Shanghai 200240, China
**wzou@sjtu.edu.cn*

Abstract: This paper proposes a novel reflectometry based on the frequency modulation pulse-compression technology, called optical pulse compression reflectometry (OPCR). Linear frequency modulation (LFM) pulse is taken as an example to implement the OPCR. Its working principle and theoretical analysis are demonstrated. The spatial resolution is determined by the sweeping range of the LFM rather than the pulse width, which overcomes the tradeoff between spatial resolution and measurement range in the conventional pulse-based optical time domain reflectometry. The influence of the laser's phase noise on the integrated side lobe ratio and peak side lobe ratio is theoretically studied. Thanks to the continuous acquisition nature of the OPCR, time averaging is valid to eliminate the influence and results in the measurement range of the OPCR beyond a few times of the source coherent length. A proof-of-concept experiment of the OPCR is carried out to verify the spatial resolution and measurement range.

OCIS codes: (060.2370) Fiber optics sensors; (060.2630) Frequency modulation; (120.4825) Optical time domain reflectometry.

References and links

1. M. K. Barnoski, M. D. Rourke, S. M. Jensen, and R. T. Melville, "Optical time domain reflectometer," Appl. Opt. **16**(9), 2375–2379 (1977).
2. X. Bao and L. Chen, "Recent progress in distributed fiber optic sensors," Sensors (Basel) **12**(12), 8601–8639 (2012).
3. W. Eickhoff and R. Ulrich, "Optical frequency domain reflectometry in single-mode fiber," Appl. Phys. Lett. **39**(9), 693–695 (1981).
4. D. Uttam and B. Culshaw, "Precision time domain reflectometry in optical fiber systems using a frequency modulated continuous wave ranging technique," J. Lightwave Technol. **3**(5), 971–977 (1985).
5. B. Soller, D. Gifford, M. Wolfe, and M. Froggatt, "High resolution optical frequency domain reflectometry for characterization of components and assemblies," Opt. Express **13**(2), 666–674 (2005).
6. S. Venkatesh and W. V. Sorin, "Phase noise considerations in coherent optical FMCW reflectometry," J. Lightwave Technol. **11**(10), 1694–1700 (1993).
7. X. Fan, Y. Koshikiya, and F. Ito, "Phase-noise-compensated optical frequency domain reflectometry with measurement range beyond laser coherence length realized using concatenative reference method," Opt. Lett. **32**(22), 3227–3229 (2007).
8. X. Fan, Y. Koshikiya, and F. Ito, "Phase-noise-compensated optical frequency-domain reflectometry," J. Quantum Electron. **45**(6), 594–602 (2009).
9. F. Ito, X. Fan, and Y. Koshikiya, "Long-range coherent OFDR with light source phase noise compensation," J. Lightwave Technol. **30**(8), 1015–1024 (2012).
10. M. A. Richards, *Fundamentals of Radar Signal Processing* (McGraw-Hill Education, 2005).
11. S. Yang, W. Zou, X. Long, and J. Chen, ""Pulse-compression optical time domain reflectometer," in the 23rd International Conference on Optical Fiber Sensors," Proc. SPIE **9157**, 915736 (2014).
12. P. Healey, "Pulse compression coding in optical time domain reflectometry," in *Proc. 7th Eur. Conf. Opt. Comun.* (1981), pp. 5.2–1.
13. M. Nazarathy, S. A. Newton, R. P. Giffard, D. S. Moberly, F. Sischka, W. R. Trutna, and S. Foster, "Real-time long range complementary correlation optical time domain reflectometer," J. Lightwave Technol. **7**(1), 24–38 (1989).
14. R. Goldman, A. Agmon, and M. Nazarathy, "Direct detection and coherent optical time-domain reflectometry with Golay complementary codes," J. Lightwave Technol. **31**(13), 2207–2222 (2013).

#224578 - $15.00 USD Received 9 Oct 2014; revised 15 Dec 2014; accepted 21 Dec 2014; published 9 Jan 2015

15. M. A. Soto, G. Bolognini, and F. Di Pasquale, "Analysis of optical pulse coding in spontaneous Brillouin-based distributed temperature sensors," Opt. Express **16**(23), 19097–19111 (2008).
16. K. Kikuchi, "Coherent optical communications: historical perspectives and future directions," *High Spectral Density Optical Communication Technologies*. (Springer Berlin Heidelberg, 2010).
17. A. Hartog and M. P. Gold, "On the theory of backscattering in single-mode optical fibers," J. Lightwave Technol. **2**(2), 76–82 (1984).
18. A. Moreira, "Real-time synthetic aperture radar (SAR) processing with a new subaperture approach," IEEE Trans. Geosci. Rem. Sens. **30**(4), 714–722 (1992).
19. N. Levanon and E. Mozeson, *Radar Signals* (John Wiley & Sons, 2004).
20. J. Armstrong, "Theory of interferometric analysis of laser phase noise," J. Opt. Soc. Am. **56**(8), 1024–1028 (1966).
21. R. Tkach and A. R. Chraplyvy, "Phase noise and linewidth in an InGaAsP DFB laser," J. Lightwave Technol. **4**(11), 1711–1716 (1986).
22. K. Aoyama, K. Nakagawa, and T. Itoh, "Optical time domain reflectometry in a single-mode fiber," J. Quant. Electron. **17**(6), 862–868 (1981).
23. L. R. Varshney and D. Thomas, "Side lobe reduction for match filter range processing," in *Radar Conference, 2003. Proceedings of the 2003 IEEE* (2003), pp.446–451.
24. M. Kashiwagi and K. Hotate, "Long range and high resolution reflectometry by synthesis of optical coherence function at region beyond the coherence length," IEICE Electron. Express **6**(8), 497–503 (2009).
25. L. Maleki, "Sources: The optoelectronic oscillator," Nat. Photonics **5**(12), 728–730 (2011).
26. F. J. Duarte, *Tunable Lasers Handbook* (Academic Press Inc., 1995).
27. T. Kurashima, T. Horiguchi, H. Izumita, S. Furukawa, and Y. Koyamada, "Brillouin optical-fiber time domain reflectometry," IEICE Trans. Commun. **76**, 382–390 (1993).
28. Y. Mizuno, W. Zou, Z. He, and K. Hotate, "Proposal of Brillouin optical correlation-domain reflectometry (BOCDR)," Opt. Express **16**(16), 12148–12153 (2008).

1. Introduction

It is well-known that optical time domain reflectometry (OTDR) can detect disturbance of optical fibers based on the-flight-of-the-pulse [1,2]. The spatial resolution of a conventional OTDR is directly determined by the pulse width. Higher spatial resolution requires narrower pulse width, which results in limited dynamic range and measurement range due to the decreased pulse energy. In order to break this limitation, optical frequency domain reflectometry (OFDR) was proposed [2–5]. OFDR uses periodical linear frequency modulation (LFM) light as the source and analyzes the back scattering light in frequency domain. The spatial resolution of OFDR is determined by the LFM sweeping range rather than the pulse width, which solves to a certain extent the dilemma of spatial resolution and dynamic range. However, its measurement range is physically limited by the laser source's coherent length [4,6]. In order to solve this issue, phase-noise-compensated OFDR (PNC-OFDR) has been introduced recently [7–9]. It adds another reference interferometer to sense the phase noise and then ensure the measurement range beyond the source's coherent length. In such systems, the performance improvement is obtained at the cost of complicated and expensive optical implementation.

This paper presents a novel reflectometry called optical pulse compression reflectometry (OPCR), which is inspired by the concept of pulse-compression radar [10,11]. It can break the limitation in conventional OTDR and OFDR with simpler optical implementation. The proposed OPCR makes use of the frequency-modulation-based pulse-compression technology. Though the impulse-like response is similar to the phase-coded OTDR [12–14] or Brillouin OTDR [15], the realization and performance are significantly different. The paper is organized as follows. In Section 2, we introduce the basic principle of FM pulse compression technology. The linear frequency modulation (LFM) pulse is taken as an example to implement the OPCR. Theoretical analysis on the spatial resolution, signal-to-noise ratio (SNR), integrated side lobe ratio (ISLR), peak side lobe ratio (PSLR), and measurement range is demonstrated. In Section 3, a proof-of-concept experiment is demonstrated to verify the theoretical analysis. Finally, a concluding remark is given.

#224578 - $15.00 USD Received 9 Oct 2014; revised 15 Dec 2014; accepted 21 Dec 2014; published 9 Jan 2015

2. Principle and theoretical analysis

2.1 Pulse compression with frequency modulation

Figure 1 depicts the general principle of FM based pulse compression technology and the initial FM pulse gets compressed by going through a matched filter. Denoting the initial FM pulse as $x(t)$ and the response of matched filter as $h(t)$, we have the following relation in time domain and frequency domain [10,11]:

$$h(t) = x^*(-t) \overset{\mathcal{F}}{\leftrightarrow} H(\omega) = X^*(\omega), \tag{1}$$

where F represents the Fourier transform; the superscript of "*" denotes the conjugation operation; $H(\omega)$ and $X(\omega)$ are the Fourier transform of $x(t)$ and $h(t)$, respectively.

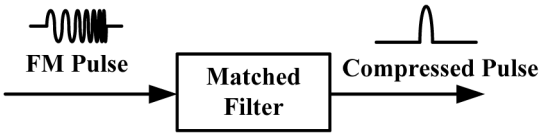

Fig. 1. Basic principle of pulse compression with frequency modulation (FM).

The Fourier transform of the output pulse $y(t)$, i.e. $Y(\omega)$, has the expression as,

$$Y(\omega) = X(\omega)H(\omega) = |X(\omega)|^2, \tag{2}$$

which demonstrates that as soon as the time-bandwidth product of the FM pulse is large enough (generally larger than 100), the output pulse is highly compressed (i.e. the impulse-like response) and its duration only depends on the bandwidth rather than its initial pulse duration. There are several kinds of pulse compression methods, such as LFM, nonlinear frequency modulation (NLFM), phase-coded modulation, etc [10]. In this work, the simple and easy one, the LFM pulse, is taken as an example to implement the proposed OPCR. Note that the phase-coded OTDR presented in [12–14] can be generalized as another type of OPCR since it is also determined by the same principle defined in Eq. (2) but depends on the phase-coding-based pulse compression technology [10].

2.2 OPCR with LFM

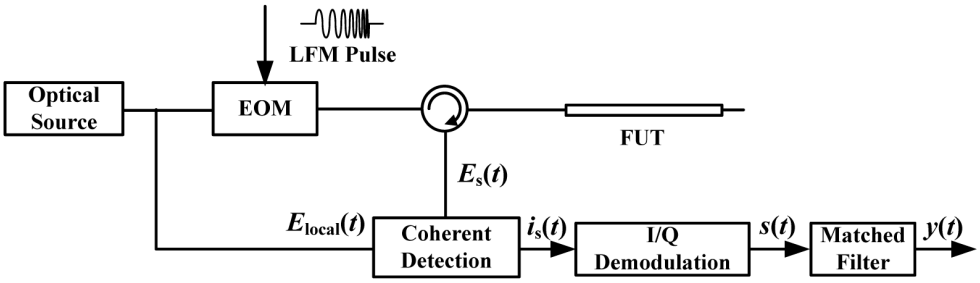

Fig. 2. Schematic configuration of OPCR based on LFM pulse compression technology. EOM: electro-optic modulator, FUT: fiber under test.

Figure 2 illustrates the schematic configuration of OPCR based on the LFM pulse compression technology. An optical source (i.e. a narrowband laser) is split into two branches: one is modulated by an LFM pulse served as the detection light towards a long optical fiber under test (FUT); the other one works as the local reference light. The backscattered light of the FUT is coherently detected together with the local reference light. The electrical signal converted by a photodetecter (PD) can be in-phase and quadrature (I/Q) demodulated by

#224578 - $15.00 USD Received 9 Oct 2014; revised 15 Dec 2014; accepted 21 Dec 2014; published 9 Jan 2015

digital processing [10] or analog processing similar to optical coherent communication technology [16]. Later, the I/Q demodulated signal goes through a matched filter to recover the backscattered light of Rayleigh scattering and/or end reflection in an FUT.

2.2.1 Spatial resolution and signal-to-noise ratio

The backscattered light E_s and the local reference light E_{local} can be expressed by:

$$\begin{aligned} E_s(t) &= A_1(t) * \left\{ rect\left(\frac{t}{T}\right) \exp\left[j2\pi f_c(t) + j\pi K t^2 \right] \right\}, \\ E_{local}(t) &= A_2 \exp\left(j2\pi f_c t \right), \end{aligned} \tag{3}$$

where $A_1(t)$ is the amplitude function of the backscattered light, the symbol of "*" stands for the convolution operation, $rect(\cdot)$ denotes the rectangular function, T is the pulse width or duration, f_c is the frequency of the carrier light, K is the LFM slope, and A_2 is the amplitude of the local reference light.

After coherent detection, the photocurrent generated from the PD is given by

$$i_s(t) \propto 2\Re \operatorname{Re}\left\{ E_s E_{local}^* \right\} = 2\Re A_2 \int_0^{T_s} A_1(\tau) rect\left(\frac{t-\tau}{T}\right) \cos\left[\pi K (t-\tau)^2 - 2\pi f_c \tau \right] d\tau, \tag{4}$$

where $\Re$ is the PD's response, τ is the round-trip propagation delay of the backscattered light in the fiber, T_s is the total round-trip propagation duration for a light going forth and back in the fiber, and $\operatorname{Re}\{\cdot\}$ denotes the real part of a complex quantity.

Using I/Q demodulation to convert a real signal to a complex one, one obtains

$$\begin{aligned} s(t) &= A(t) * x(t), \\ A(t) &= 2\Re A_2 A_1(\tau) \exp(-j2\pi f_c \tau), \\ x(t) &= \left\{ rect\left(\frac{t}{T}\right) \exp\left[j\pi K t^2 \right] \right\}. \end{aligned} \tag{5}$$

The impulse response of the matched filter is determined by

$$h(t) = x^*(-t) = rect\left(-\frac{t}{T}\right) \exp\left(-j\pi K t^2\right). \tag{6}$$

After the matched filtering process [i.e. the convolution between Eq. (5) and Eq. (6)], the effective signal can be expressed as

$$\begin{aligned} y(t) &= s(t) * h(t) = [A(t) * x(t)] * h(t) = A(t) * [x(t) * h(t)] = A(t) * C(t), \\ C(t) &= x(t) * h(t) = \left\{ rect\left(\frac{t}{2T}\right) \frac{T \sin\left[\pi K (T - |t|)(t) \right]}{\pi K T(t)} \right\}, \end{aligned} \tag{7}$$

where $C(t)$ denotes the waveform of the compressed pulse.

Numerical simulations of the pulse compression for a single pulse at $\tau = 0$ are shown in Fig. 3. The original LFM pulse [see Fig. 3(a)] is compressed as a narrow sinc-like pulse [see Fig. 3(b)] by the matched filtering process. The full width at half maximum (FWHM) or 3 dB width of the main lobe is determined by $1/KT$. In theory, the spatial resolution of a reflectometry is defined as the one-way propagation distance within a half of the FWHM, which can be written as

#224578 - $15.00 USD Received 9 Oct 2014; revised 15 Dec 2014; accepted 21 Dec 2014; published 9 Jan 2015

$$R = \frac{c}{2nKT} = \frac{c}{2nB}, \tag{8}$$

where c is the light speed in vacuum, n is the refractive index of the FUT, and $B = KT$ is the LFM sweeping range. Equation (8) shows that the spatial resolution of the OPCR is now determined by B instead of the pulse's intrinsic width, which physically breaks the restriction between spatial resolution and measurement range. It is worth noting that there are high-level side lobes in the compressed pulse [see Fig. 3(c)], which may affect the performance of the OPCR as will be discussed below.

Provided the Gaussian white noise with a power spectral density N_0 (in unit of W/Hz or W·s) is considered, which is mainly limited by the thermal noise of the photo-detector, the signal-to-noise ratio (SNR) of the OPCR after the matched-filtering process is determined by

$$SNR \propto \frac{P_s}{N_0}, \tag{9}$$

where P_s (in unit of W·s) represents the total energy of a LFM pulse with the pulse width or duration of T. If the peak power level of the pulse is constant (P_{pk}), $P_s = T \cdot P_{pk}$. It means that P_s is proportional to the pulse width T and longer T corresponds to greater P_s. Consequently, the SNR defined in Eq. (9) can be greatly improved by simple use of a longer pulse width.

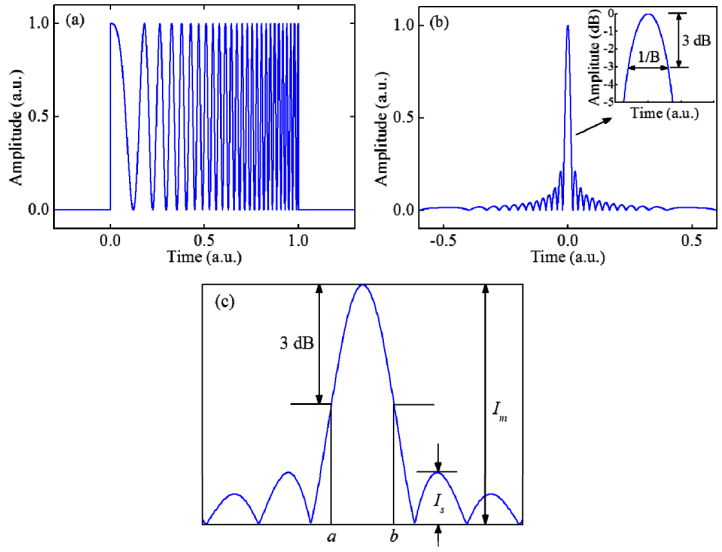

Fig. 3. Qualitative description of pulse-compression process. (a) Time-domain profile of LFM pulse and (b) compressed pulse with a 3-dB width equal to 1/KT. (c) Zoomed-in compressed pulse for definition of two parameters of ISLR and PSLR.

2.2.2 Integrated side lobe ratio and peak side lobe ratio

According to Eq. (7), the effective signal of the OPCR is determined by the convolution of the compressed pulse $C(t)$ and the backscattered light $A(t)$. $A(t)$ includes Rayleigh backscattering occurring anywhere in the entire FUT, splicing loss at particular points, end reflection due to Fresnel reflection [17]. Therefore, the performance of the OPCR should be significantly influenced by the side lobes of the compressed pulse. Here, we introduce two important parameters, nominated integrated side lobe ratio (ISLR) and peak side lobe ratio (PSLR), which are also key parameters in modern Radars [18,19]. In mathematics, both ISLR and PSLR are represented by [18,19]

#224578 - $15.00 USD Received 9 Oct 2014; revised 15 Dec 2014; accepted 21 Dec 2014; published 9 Jan 2015

$$ISLR = 10\log_{10}\frac{\int_a^b |C(\tau)|^2 d\tau}{\int_{-\infty}^a |C(\tau)|^2 d\tau + \int_b^\infty |C(\tau)|^2 d\tau},$$
$$PSLR = 10\log_{10}\frac{I_m}{I_s}, \quad (10)$$

where $[a, b]$ denotes the 3-dB region around the main lobe and I_s (I_m) corresponds to the peak intensity of the highest side lobe (main lobe), as illustrated in Fig. 3(c). In physics, the ISLR is the ratio of the power in the main lobe to the total power in all the side lobes. It characterizes the ability of the OPCR to detect weak reflection buried in the total backscattered light. The PSLR is defined by the ratio of the largest amplitude of side lobes to the peak of main lobe. It represents the capacity of the OPCR to identify a weak reflection from a nearby strong reflection. As will be introduced in Session 3, a long FUT with two peaks prepared at the far end and artificially loosely connected with each other is designed to verify the ISLR and PSLR of the OPCR.

2.2.3 Influence of phase noise

Since the laser source always suffers random phase fluctuation, called phase noise [20,21], Eq. (3) should be modified as

$$E_s'(t) = A_1(t) * \left\{ rect\left(\frac{t}{T}\right) \exp\left[j2\pi f_c(t) + j\pi K t^2 + j\phi(t) \right] \right\},$$
$$E_{local}'(t) = A_2 \exp\left[j2\pi f_c t + j\phi(t) \right], \quad (11)$$

where $\phi(t)$ is the phase noise. The signal after coherent detection and I/Q demodulation turns to

$$s'(t) = \int_0^{T_s} A(\tau) x_\tau(t) d\tau,$$
$$x_\tau(t) = x(t-\tau) \exp\left[j\phi(t) - j\phi(t-\tau) \right], \quad (12)$$

where $x_\tau(t)$ denotes the LFM pulse at the delay of τ when the phase noise is considered.

The phase change of the optical source over time τ can be assumed to be a stationary zero-mean variable so that the phase change in different time t is statistically independent [20]. The original and compressed pulses at the delay of τ can be expressed by

$$x_\tau(t) = rect\left(\frac{t-\tau}{T}\right) \exp\left[j\pi K (t-\tau)^2 \right] \exp\left[j\Delta\phi(\tau) \right],$$
$$C_\tau(t) = x_\tau(t) * h(t) = C(t) \exp\left[j\Delta\phi(\tau) \right]. \quad (13)$$

where $\Delta\phi(\tau) = \phi(t)$-$\phi(t$-$\tau)$. Provided a Lorentzian source, the distribution of random phase change $\Delta\phi(\tau)$ satisfies the Gaussian distribution with deviation $\sigma^2(\tau) = 2\pi|\tau|\Delta\nu = 2\tau/\tau_c$, where $\Delta\nu$ is the linewidth and τ_c is the coherent time of the source [21].

#224578 - $15.00 USD Received 9 Oct 2014; revised 15 Dec 2014; accepted 21 Dec 2014; published 9 Jan 2015

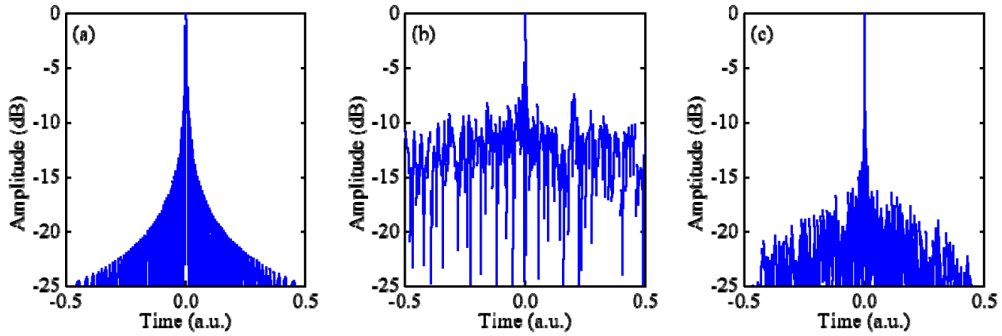

Fig. 4. Numerical simulation of the influence of phase noise. The compressed pulse without (a) and with (b) phase noise. (c) The compressed pulse after 10,000 time averaging.

Figure 4 depicts the numerical simulation of the influence of phase noise ($\tau/\tau_c = 5$) on the waveform of the compressed pulse. A clear comparison between Figs. 4(a) and 4(b) demonstrates that the waveform of the compressed pulse is seriously disturbed by the phase noise. This is because the matched filter [see Eq. (6)] is free from the phase disturbance so that the compressed pulse $C_\tau(t)$ in Eq. (13) becomes very sensitive to the phase noise. Thanks to the continuous acquisition nature of the proposed OPCR, which is in principle similar to the OTDR [1,22], time averaging process is sufficient to overcome the phase disturbance. Figure 4(c) shows the simulated result after 10,000 averaging. In contrast, the signal in OFDR is achieved by real-time acquisition and fast Fourier transform [3], corresponding to the transient backscattered light. It cannot be overwhelmed by time averaging and thus limits the maximum measurement range no larger than a half of the source's coherent length [4,5].

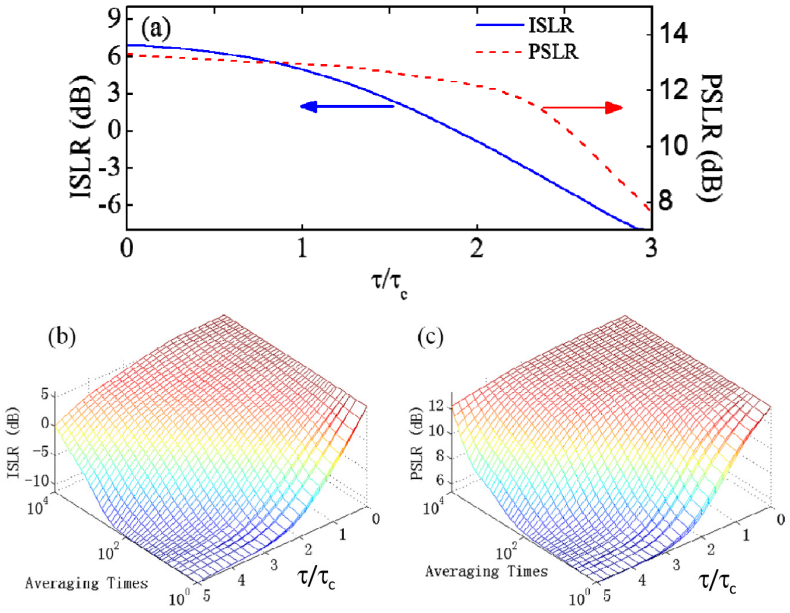

Fig. 5. (a) Dependence of both ISLR and PSLR on the phase noise. The effect of time-averaging process on (b) ISLR and (c) PSLR.

Next, we study the influence of the phase noise on the ISLR and PSLR of the OPCR. As shown in Fig. 5(a), both ISLR and PSLR are sharply decreased and thus the detection ability (i.e. the measurement range) of the OPCR is significantly reduced if the phase noise (or τ/τ_c) becomes larger. Figures 5(b) and 5(c) illustrates that time averaging process is also useful for

#224578 - $15.00 USD Received 9 Oct 2014; revised 15 Dec 2014; accepted 21 Dec 2014; published 9 Jan 2015

improvement of both ISLR and PSLR. Besides, more times of averaging are required for much longer measurement range (i.e. greater τ/τ_c). Note that the additional effect of the pulse duration on the influence of the phase noise is now under study.

3. Experimental demonstration

The proof-of-concept experiment of the OPCR system is carried out and its setup is depicted in Fig. 6. A 1550 nm distributed feedback laser diode (DFB-LD, NEL NLK1C6DAAA) with 100 kHz linewidth is used as the optical source. A voltage-controlled oscillator (VCO, Minicircuits ZX95-2536C) with 221 MHz sweeping range from 2.315 GHz to 2.536 GHz is driven by a sawtooth wave with 2 μs period to generate periodical LFM signal. The VCO is connected to a single sideband modulator (SSBM) and the LFM spectrum of the VCO [see the inset of (a) of Fig. 6] is measured by an electric spectrum analyzer. Note that the LFM spectrum deviates slightly from a typical flat LFM spectrum (especially at the high frequency of 2.536 GHz) because the amplitude of the VCO during scanning is distorted. This deviation is essentially compensated since a broadband amplifier (Minicircuits ZX60-272LN +) is laid after the VCO and before driving the SSBM. The SSBM modulates one beam of the DFB-LD to get either the upshifted or downshifted sideband that is in frequency away from the DFB-LD. In consequence, the frequency change of the VCO leads to the same change of the modulated sideband and thus a periodical LFM light is generated. This light is further modulated by a MZM with a square pulse with 2 μs duration, as the period of LFM signal, and 1 ms period so as to turn the periodical LFM light to a pulsed LFM light. Note that the pulsed LFM light after the MZM is additionally used for time averaging measurement. The sawtooth wave and square pulse are strictly synchronous since both are generated by the same arbitrary waveform generator (Agilent 81150A). Two erbium-doped fiber amplifiers (EDFAs) are used to compensate the loss of SSBM and MZM, respectively. Note that the EDFA laid between the SSBM and MZM is a two-stage EDFA with an optical filter installed inside. The average optical power launched into the FUT is ~20 dBm.

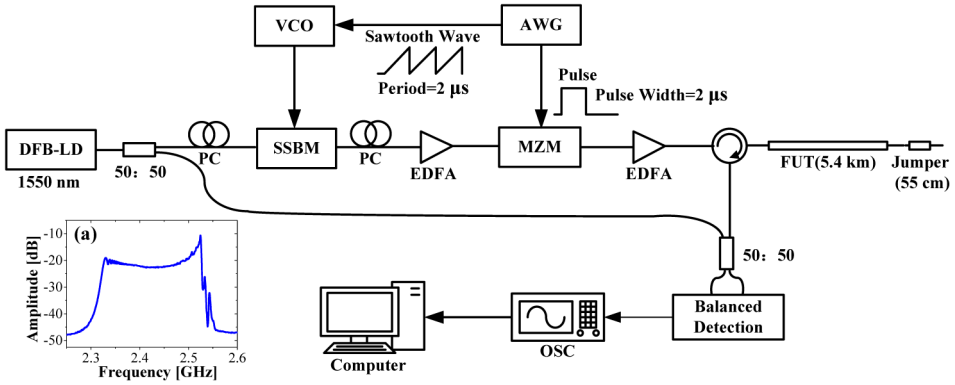

Fig. 6. Proof-of-concept experiment of the OPCR system. The inset (a) shows the LFM spectrum with 221 MHz sweeping range. DFB-LD: distributed feedback laser diode, SSBM: single sideband modulator, VCO: voltage-controlled oscillator, AWG: arbitrary waveform generator, MZM: Mach-Zehnder modulator, PC: polarization control, EDFA: Erbium-doped fiber amplifier, OSC: oscilloscope.

The coherent detection of the backscattered light is realized by two steps. First, a 50:50 coupler is used for heterodyne detection between the backscattered light and the other part of the DFB-LD (~7 dBm power) that serves as the local reference light. Second, two outputs of the coupler are detected by a balanced PD (Discovery DSC720) with 16 GHz bandwidth. An oscilloscope is used to collect the electrical signal of the balanced PD. The I/Q demodulation and matched filtering are numerically fulfilled by computer software as referred to [10]. For verifying the spatial resolution, a 55 cm jumper is loosely connected with the far end of 5.4

#224578 - $15.00 USD Received 9 Oct 2014; revised 15 Dec 2014; accepted 21 Dec 2014; published 9 Jan 2015

km FUT by a set of fiber adaptors (FC/UPC). Note that this connection is artificially processed so as to let both the far end of the FUT and the end of the jumper generate Fresnel reflection. However, this artificial process is hard to equalize the two reflections.

The proof-of-concept measurement with 1,000 averages is depicted in Fig. 7(a), which shows that the OPCR can successfully detect Fresnel reflection at the far end of the FUT. More detail of the far end of the FUT is illustrated in the right inset of Fig. 7(a). There are two peaks separated by 55-cm-long interval. It verifies the nominal spatial resolution of 47 cm, which is deduced by substituting B = 221 MHz and n = 1.446 into Eq. (8). The FUT's length (~5.4 km) is 2.7 times of the source's coherent length (~2 km), identifying τ_{max}/τ_c = 5.4 and confirming the theory that the OPCR can go far beyond the coherence length after time averaging over numerous repeating measurement. However, there is more or less amplitude fluctuation existing in the entire curve. A numerical simulation of the backscattered curve is compared in Fig. 7(b). The simulation is in a reasonable match with the experimental observation in Fig. 7(b). The amplitude fluctuation is mainly due to the limited ISLR of the OPCR based on LFM since Rayleigh scattering occurs anyway of the FUT. Besides, compared with the simulation result, the right peak at the far end of the FUT in the experimental result is quite lower than the left peak. This is because the artificial connection of the 55 cm jumper cannot ensure two equal reflections and the PSLR of the OPCR is not high enough. In the future study, we will prepare a better FUT with approximately equal ending reflections and further utilize the proper windowing (i.e. apodization) or NLM [19,23] into the OPCR so as to probably reduce the amplitudes of the side lobes and potentially eliminate their influences to the ISLR and PSLR (i.e. the performance) of the OPCR.

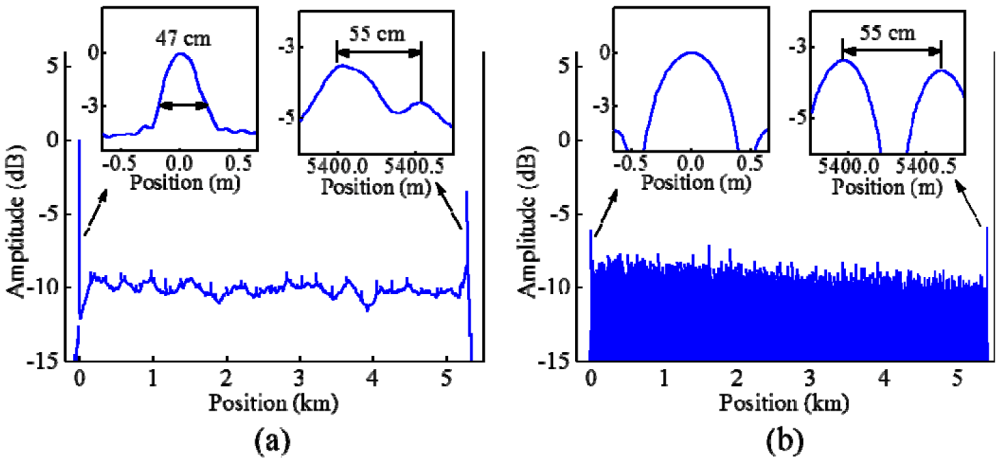

Fig. 7. Comparison between the proof-of-concept measurement (a) and numerical simulation (b). The insets show the magnified curves at the near and far ends of the FUT, respectively.

Moreover, as shown in the left inset of either Fig. 7(a) or Fig. 7(b), there is a "ghost" peak at the beginning of the FUT although the FUT is spliced with the port 2 of the circulator in Fig. 6. Figure 8 explains the causes for the "ghost" peak. As mentioned above [see Eq. (7)], the OPCR signal after matched filtering is essentially the convolution of the intrinsic reflection trace [see Fig. 8(a)] and the compressed pulse [see Fig. 8(b)]. The convolution can be decomposed as the accumulation of the compressed pulse at different delays. Figures 8(c) and 8(d) demonstrate the accumulation process of the real component and imaginary component of the signals, respectively. For a fixed point corresponding to a time delay of τ_0 ($\tau_0 \geq 0$), its OPCR signal is mainly affected by the main lobe of the compressed pulse at τ_0 and the side lobes from the compressed pulses before or after τ_0. Since there is no any backscattered light before the port 2 of the circulator (i.e. the beginning of the FUT or τ = 0),

#224578 - $15.00 USD Received 9 Oct 2014; revised 15 Dec 2014; accepted 21 Dec 2014; published 9 Jan 2015

the influence introduced by the side lobes only come from the delays after $\tau = 0$ (i.e. $\tau \geq 0$). The real component, imaginary component, and amplitude of the convoluted signals are shown in Figs. 8(e), 8(f) and 8(g), respectively. It explains why the "ghost" peak appears at the beginning of the trace although it does not correspond to a real strong reflection.

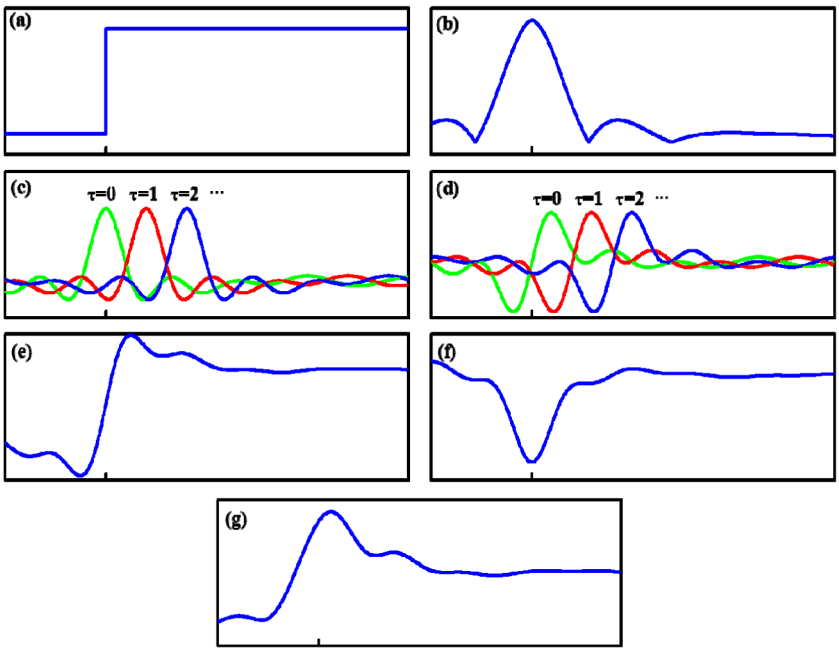

Fig. 8. (a) Schematic of the ideal backscattered trace starting at $\tau = 0$ (i.e. the location of the circulator in Fig. 6) where no any reflection exists except for Rayleigh backscatter. (b) A compressed pulse to convolute the ideal backscattered trace. Demonstration of the accumulation process of the real component (c) and imaginary component (d) of the compressed pulse. The real part (e), imaginary part (f), and (g) amplitude of the OPCR's trace after matched filtering.

4. Conclusion

We have demonstrated a new type of reflectometry based on the FM pulse compression technology, nominated OPCR. The working principle and theoretical analysis of an OPCR with LFM pulse as an example shows that the spatial resolution is only determined by the LFM sweeping range instead of the pulse width. The measurement range of the OPCR can be beyond a few times of the source coherent length by time averaging, which is similar with the conventional OTDR. Although the phase noise of the laser source has strong influence to the compressed pulse as well as the ISLR and PSLR of the OPCR, the influence can be effectively eliminated if the time averaging is sufficient. Furthermore, the optical implementation remains the same complexity as the traditional OFDR, but is much simpler than the PNC-OFDR. A proof-of-concept experiment of the OPCR verifies that the spatial resolution of 47 cm with 221 MHz sweeping range is far better than that of OTDR using 2 μs pulse duration and the measurement range of 5.4 km is beyond the source's coherent length by 2.7 times.

Compared with the reflectometry based on the synthesis of optical coherence function [24], the measurement range of the OPCR beyond the coherence length is more easily achieved. The current performance (measurement range and/or spatial resolution) of the proof-of-concept OPCR is still less than the state of the arts of OTDR [2] and OFDR [5] or

#224578 - $15.00 USD Received 9 Oct 2014; revised 15 Dec 2014; accepted 21 Dec 2014; published 9 Jan 2015

PNC-OFDR [9] because of the experimental conditions (the limited sweeping range of the VCO and coherence length of the laser source). Besides, more efforts are also required to optimize the LFM in the OPCR by use of proper windowing (i.e. apodization) or NLM [19,23]. However, as theoretically proved in this work, the spatial resolution of the OPCR is only related to the compressed pulse (i.e. sweeping frequency range) and the measurement range can be extended beyond the source's coherent length through sufficient time averaging. Therefore, a high spatial resolution and long measurement range of the OPCR, which is comparable to or even better than [2,5,9], is highly expectable if the VCO is replaced by an opto-electronic oscillator (OEO) with wider sweeping frequency range [25] and a more stable diode or fiber laser [26] substitutes for the DFB-LD. Moreover, the inspiration of the proposed OPCR may boost development of Brillouin-based distributed optical fiber sensors [15,27,28] with no tradeoff between the spatial resolution and measurement range.

Acknowledgment

This work was partially supported by National Natural Science Foundation of China (61007052 and 61127016), SRFDP of MOE (Grant No. 20130073130005), and the State Key Lab Project of Shanghai Jiao Tong University (GKZD030033).

#224578 - $15.00 USD Received 9 Oct 2014; revised 15 Dec 2014; accepted 21 Dec 2014; published 9 Jan 2015